Progress In Electromagnetics Research M, Vol. 111, 159–171, 2022

A Miniaturized 2 × 2 Double Flare Horn Shaped MIMO Antenna with Enhanced Isolation for K and Ka Band Applications

Aditya K. Singh*, Amrees Pandey, Piyush K. Mishra, and Ram S. Yadav

Abstract—The article presents a compact size and high isolation with 2 × 2 MIMO, double flare horn shaped antenna for K and Ka bands of mm-wave applications. The overall size of the MIMO antenna $0.19\lambda \times 0.19\lambda \times 0.01\lambda\,\text{mm}^3$ at a lower frequency has been designed, simulated, fabricated, and tested. The proposed MIMO antenna components are arranged parallel with identical shapes to provide a high level of inter-element isolation and 50 W microstrip line feed. The antenna covers 18.61–20.01 GHz in the K-band (18–26.5 GHz) and 21.52–33.91 GHz in the Ka-band (26.5–40 GHz) with impedance bandwidths of 7.2% and 44.5% respectively at port-1 and port-2. Maximum peak gain of 6.5 dBi & 8.1 dBi at port-1 and 6.5 dBi &7.9 dBi at port-2 is observed respectively. Diversity characteristics such as envelope correlation coefficient, diversity gain, total active reflection coefficient, and channel capacity loss are determined to validate the considered MIMO antenna's work qualities. The isolation of more than 35 dB indicates that the proposed structure is suitable to use a dual-port MIMO antenna. The recommended structure's investigation revealed a steady performance and a high degree of agreement between simulated and measured findings.

1. INTRODUCTION

The rapid augmentation of wireless devices, limited bandwidth (BW), and confined channel capacity have all fueled efforts to construct and emphasize communication network standards in the present period [1, 2]. As a result, the analyses of future propagation 5G communication system using the mm-wave spectrum with appreciably higher data speeds & channel capacity has been precipitated. In this sense, 5G wireless system must attain three main conditions: (i) have high throughput, (ii) have less energy consumption, (iii) serve many users simultaneously, the final being presumably the largest diving force of 5G [2, 3]. Therefore, K- and Ka-bands have further down absorptions, slighter path loss, and deceased signal fading so that Ka-band is highly advisable in millimeter BW. For 5G mm-wave, the application requires high gain and wide BW [4–6]. Many authors have considered numerous MIMO antenna designs & their conformabilities useful for mm-wave-based wireless applications ranging from [7–9].

Furthermore, the multiplexing gain is important for MIMO systems; the MIMO antenna is suitable for improving data rate transmission[10]. Experimenters are endeavoring to structure a simple antenna to prepare high mutual coupling between ports. A very compact size MIMO antenna anyhow degrades the accomplishment of antenna ports [4, 10, 11]. A lot of techniques have been proclaimed to decrease isolation in MIMO antenna system such as reflector, meta surface, diversity technique, and neutralized line. The distance between the radiating elements forms the MIMO structure; therefore, the enhanced role of MIMO antenna performance is based on the spacing between the elements [12]. Anyhow, the possible space is unsuitable for a realistic portable devices. In this way, many techniques have been adopted to lower the isolation between MIMO elements [13, 14].

Received 6 May 2022, Accepted 16 June 2022, Scheduled 13 July 2022
* Corresponding author: Aditya Kumar Singh (aditya08129@gmail.com).
The authors are with the Department of Electronics & Communication, University of Allahabad, Prayagraj, India.

Ultra-wideband (UWB) technology has been examined in data transfer at high speed, prudential cost, and better quality of services (QoS), and these are the remarkable traits of future wireless communication systems. When ultra wideband & MIMO are coupled with space multipath and parallel transmission of various signals, considerable diversity & multiplexing benefits can be achieved.

Numerous MIMO antenna structures have been recently explained in the literature for K and Ka bands of mm-wave applications [4–6]. Reference [14] describes a coplanar waveguide fed reconfigurable antenna with a multiport pattern diversity antenna for K & Ka band application. A super wideband MIMO antenna for S, C, X, K, and Ka is reported in [15] for wireless communication. In [16], a multi-element antenna design allows the radiation to bend in the desired direction, which is ideal for 5G communications In [17], UWB and low isolation of two port MIMO antenna for wireless communication have been reported. A comprehensive review of broadband, multiband, & UWB antennas as well as the materials and geometry numerical tools for wireless communication is reported [18]. ECC is also assessed in [19] to assure MIMO performance.

In the present manuscript, the design of a double flare horn shaped MIMO antenna with ultra UWB for K and Ka bands is demonstrated. Using this proposed antenna A_4 is designed to keep them identical to each other, so that radiating patch has better polarization diversity and good isolation between the double flare horn shaped antennas. The overall compact dimension of antenna is $0.19\lambda \times 0.19\lambda \times 0.01\lambda\,\text{mm}^3$, printed on an FR4 epoxy substrate ($\varepsilon_r = 4.4$, $\tan\delta = 0.02$ and thickness of 1.6 mm) and simulated by ANSYS HFSS 18 electromagnetic simulator. The main characteristics of the double flare horn shaped antenna for this paper are as follows —

(i) The two resonant frequencies of 19.65 GHz and 22.31 GHz with impedance bandwidths of 1400 MHz (18.61–20.01 GHz) and 12390 MHz (21.52–33.91 GHz) respectively are at ports $|S_{11}|$ and $|S_{22}|$. However, port $|S_{22}|$ has the same resonant frequency as port $|S_{11}|$ for K and Ka bands of mm-wave applications.

(ii) Excellent isolation is > 35 dB by the orthogonal arrangement of dual ports to maximize the inter-connection element.

(iii) The present simulated results, S-parameters, peak gain, isolation, radiation efficiency, MIMO performance parameters; ECC, DG TARC, and CCL characteristics & measurable results from the archetype fabrication are examined.

2. SCHEMATIC LAYOUT FABRICATED OF CONSIDERED ANTENNA STRUCTURE

The dimensional structure of the considered antenna has a red color (upper part) of radiating elements and green color (lower part) of the ground plane dual port MIMO antenna which is fed by a $50\,\Omega$ microstrip feed line (Figure 1). The proposed double flare horn shaped antenna is fabricated on an FR4 epoxy substrate ($\varepsilon_r = 4.4$, $\tan\delta = 0.02$,& thickness of 1.6 mm) & tested in order to validate the simulated results. The picture of the prototype antenna is used for the measurement as shown in Figure 2. All the measurements were taken using Schwarz vector Analyzer ZNB40 which operates in the frequency range of 10 MHz to 40 GHz.

The proposed double flare horn-shaped antenna is obtained. The systematic growth of A_1 to A_4 is displayed in Figure 3. Antenna-1 (A_1) is achieved by introducing two identical structures with deformed flare horn-shaped ($13.5 \times 3.5\,\text{mm}^2$) and rectangular slots ($8 \times 8\,\text{mm}^2$) of radiating elements (cf. Figure 3 and Table 1). A_2 (Antenna-2) is obtained with the help of antenna-1 which has etched parallel rectangular slots ($8\times4\,\text{mm}^2$) in radiating elements (cf. Figure 3 and Table 1). A_3 (Antenna-3) is achieved by introducing Antenna-2, which has etched parallel rectangular slots ($12 \times 2\,\text{mm}^3$) from a symmetrical overlay flare horn-shaped antenna in a conducting patch (cf. Figure 3 and Table 1). The proposed antenna (Antenna-4) is obtained from Antenna-3 which has etched one circular slot of radius 1.5 mm in middle, a portion of the radiating elements (cf. Figure 3 and Table 1). The ground geometry of these entire antennas (A_1–A_4) is the same, mutually coupled at ports-1 and 2. Two identical designs are deformed with double flare horn shape by keeping them apart from each other at an optimized distance (6 mm) of the conducting patches to create a MIMO structure of the antennas (A1–A_4), but the proposed antenna (A_4) which has increased the mutual coupling between the ports and also enhanced the gain as well as UWB. Furthermore, MIMO appearances bordering on ECC (envelope correlation

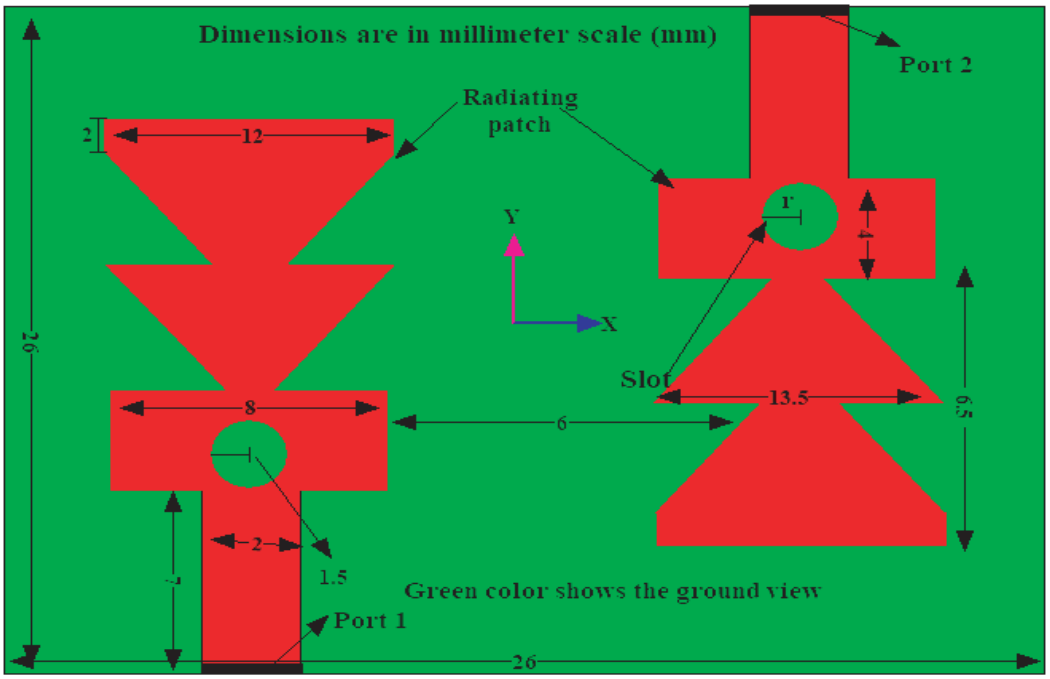

Figure 1. Antenna's frontal (red) & back (green) view.

coefficient), inclusive DG (diversity gain), TARC (total active reflection coefficient), and CLL (channel capacity loss) are analyzed by resources ANSYS HFSS 18 electromagnetic simulator.

As seen in Figure 4, the dual port proposed antenna A_4 is arranged in an identical orientation structure. Figure 4(a) illustrates the features of all the two ports return loss (18.61–20.01 GHz) and (21.52–33.91) GHz respectively with impedance bandwidth of 44.5% & gain of 8.1 dBi at $|S_{11}|$ which are almost similar, and the isolation between the two ports is more than 35 dB (cf. Figure 4(b)). These radiating elements give excellent impedance matching which covers the entire UWB, K band, and Ka band applications.

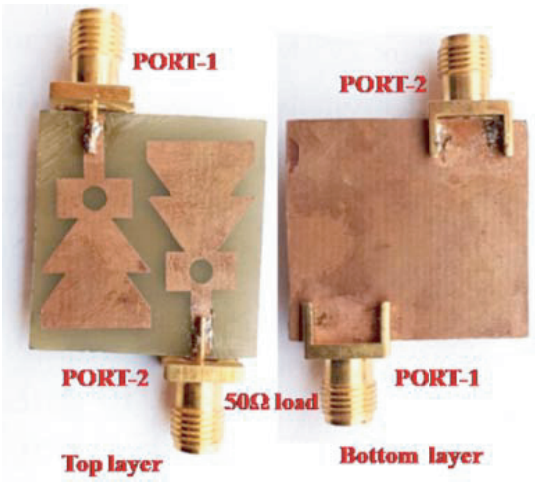

(a)

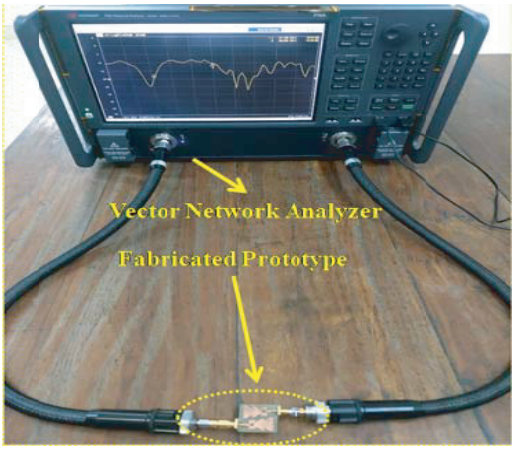

(b)

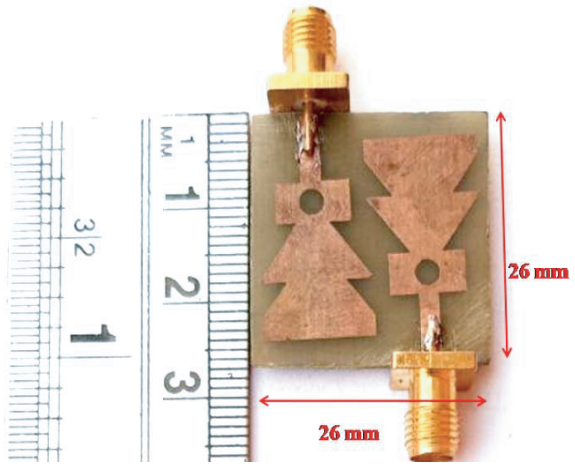

(c)

Figure 2. Fabricated archetype of the MIMO antenna. (a) Top & bottom view. (b) Measurement setup using VNA ZNB40. (c) Dimension of fabricated antenna.

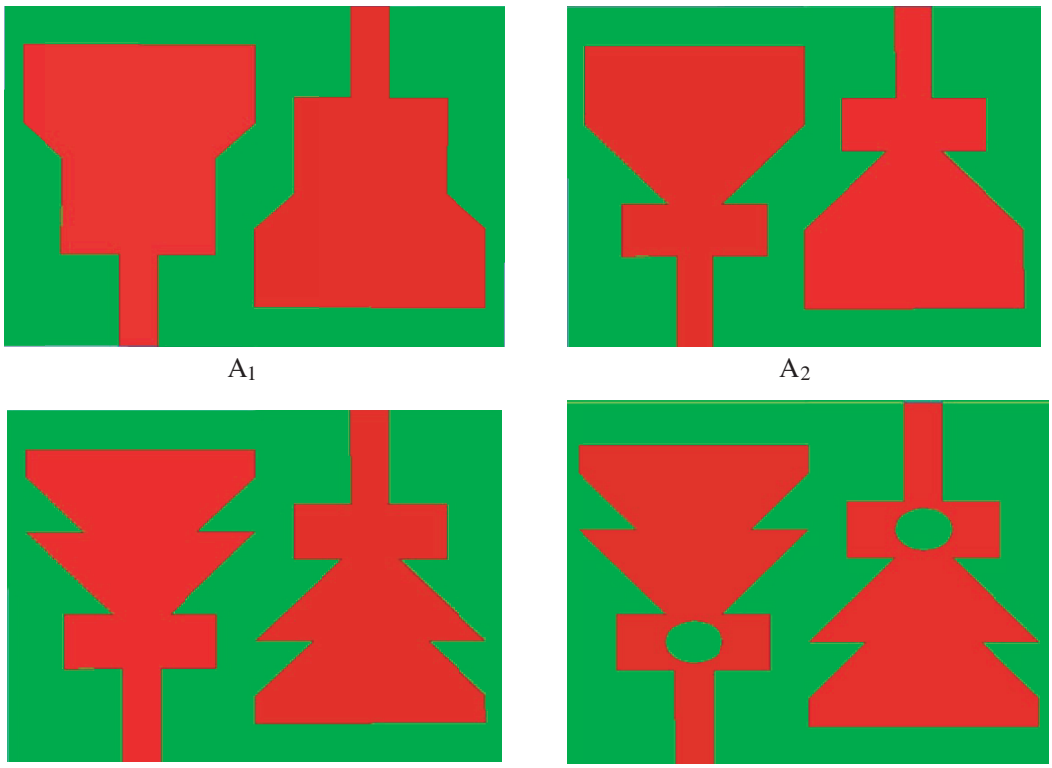

A_1 A_2

A_3 A_4

Figure 3. Step-wise antenna growth of the A_1, A_2, A_3, & A_4.

3. EXPERIMENTAL RESULTS AND VALIDATION

The double flare horn shaped antenna has been fabricated. The measurements of return loss, isolation, peak gain, TARC, VSWR, as well as CCL have been reported. It is perceived from the figure that simulated and measured results are in good agreement. In Table-1, the data in the expression of the

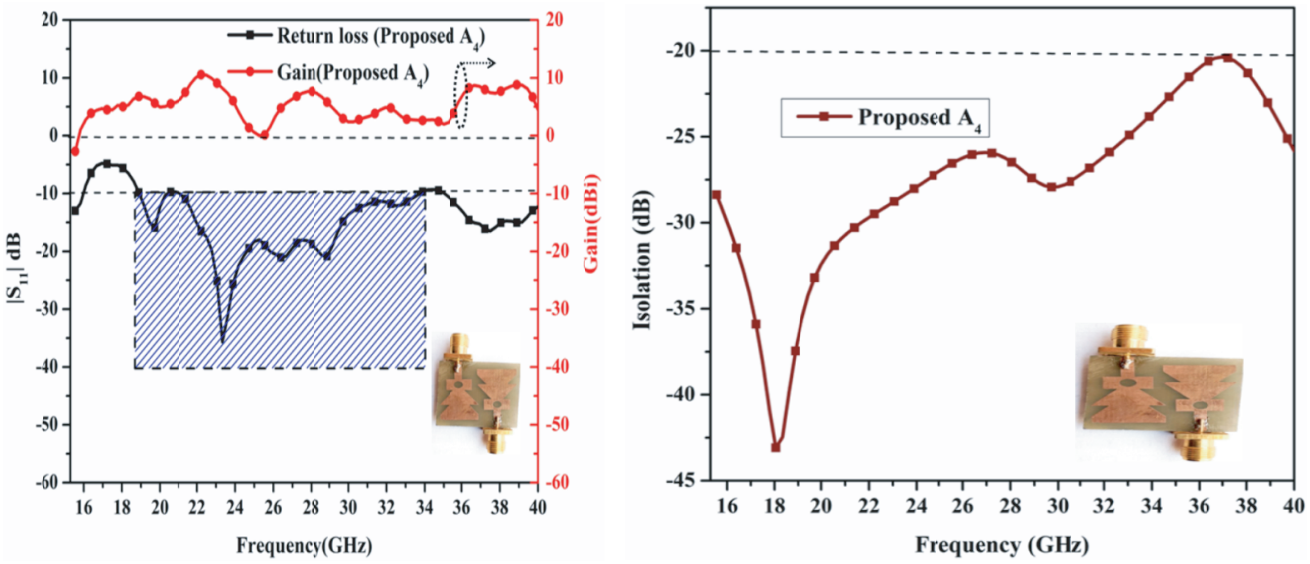

(a) (b)

Figure 4. Proposed antenna A_4. (a) Return loss. (b) Isolation.

operating band (in GHz) with impedance bandwidth (in %), resonant frequency (in GHz), return loss (in dB), and peak gain (in dBi) of antennas (A_1–A_4) at both ports, i.e., port-1 and 2 are reported.

3.1. Return Loss ($|S_{11}|$ and $|S_{22}|$) and Isolation ($|S_{12}|$ & $|S_{21}|$)

The '$|S_{11}|$', '$|S_{22}|$', '$|S_{12}|$', & '$|S_{21}|$' values of the fabricated prototype are measured using a Schwarz vector Analyzer ZNB40. Figure 5(a) illustrates two resonating bands of 18.61–20.01 GHz (simulated)/19.55–20.01 GHz (measured) and 21.52–33.91 GHz (simulated)/22.62–32.91 GHz (measured) below −10 dB emission point with impedance bandwidth of 7.2% (simulated)/6.6% (measured) and 44.5% (simulated)/42.9% (measured) respectively at port 1 (S_{11}). In Figure 5(b), port-2 ($|S_{22}|$) has the same behavior as port-1, and both show ultra-wideband characteristics, from the survey of Figures 5(a) and (b). It is perceived that the simulated and measured effects are in excellent consistency by a slight difference. More than 35 dB isolation (simulated and measured) between the antenna units for the proposed configurations makes it suitable for dual MIMO application. (cf. Figure 5(c)).

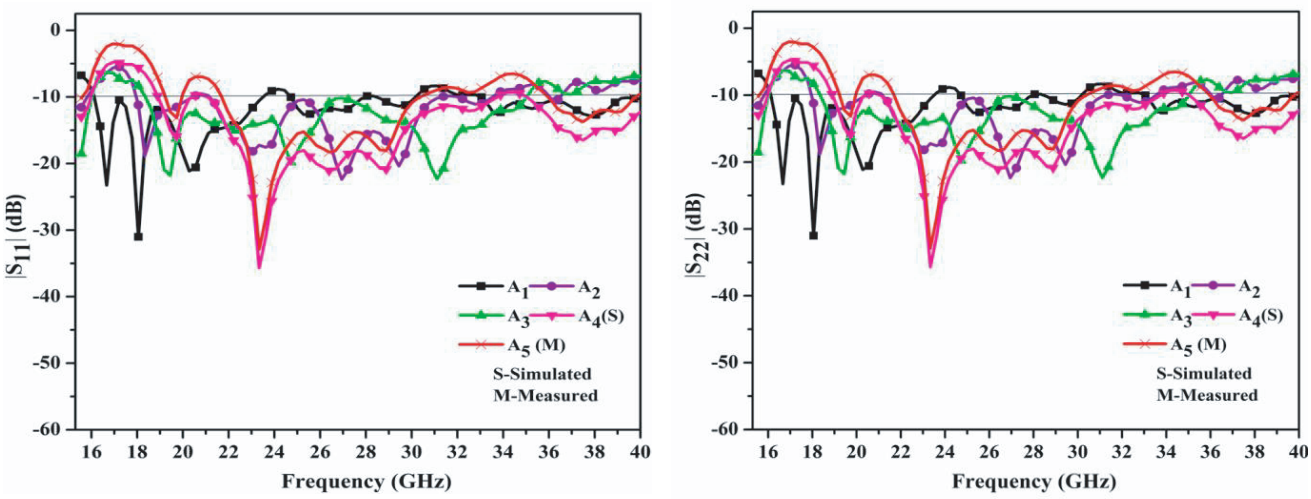

(a) (b)

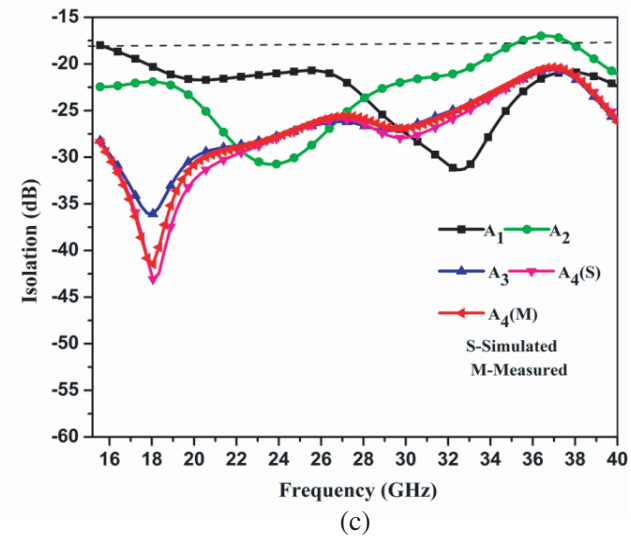

(c)

Figure 5. Simulated and Measured results in term of (a) $|S_{11}|$, (b) $|S_{22}|$, (c) isolation ($|S_{12}|$ & $|S_{21}|$ versus frequency curve of the antenna (A_1–A_4).

3.2. Scattering Parameters and Peak Gain (dBi)

The simulated and measured analyses of the proposed MIMO antenna in terms of 'S_{11}' and 'S_{22}', 'S_{12}', & 'S_{21}' are represented in the Figure 6(a) (A_1–A_4) is represented in Figure 6(b). In Table 1, we examined these antennas (A_1–A_4) and compared all these antennas, finding that the proposed antenna A_4 is superior in terms of impedance bandwidth, peak gain, and isolation. However, the designed MIMO layout has two resonating frequency bands of 18.61–20.01 GHz (simulated)/19.55–20.01 GHz (measured) and 21.52–33.91 GHz (simulated) /22.62–32.91 GHz (measured) with impedance bandwidth of 7.2% (simulated)/6.6% (measured) and 44.5% (simulated) /42.9% (measured) respectively for port-1. For MIMO, an antenna's required isolation is < -15 dB. The proposed isolation with simulated

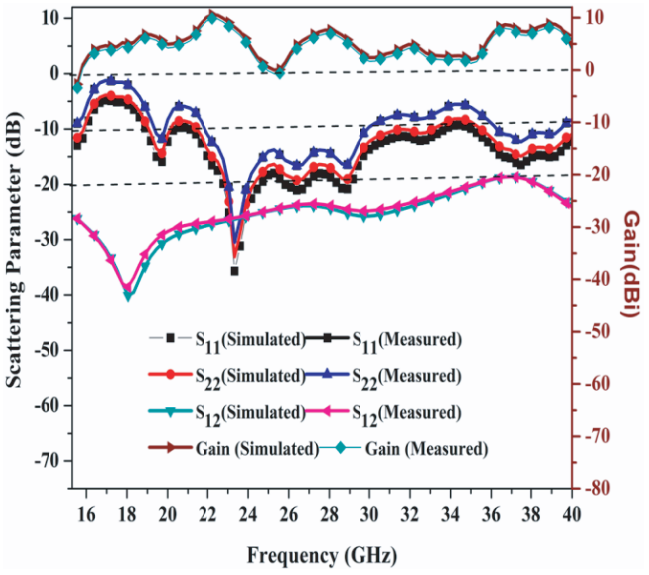

(a)

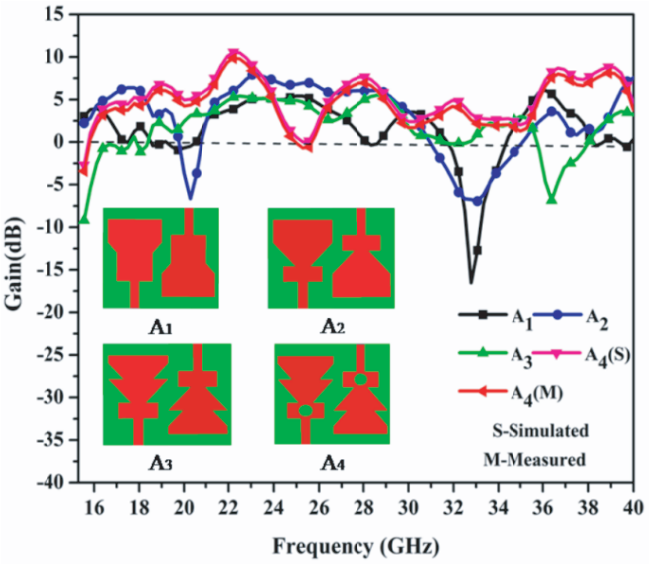

(b)

Figure 6. Simulated and Measured in term of (a) scattering parameter, (b) gain.

Table 1. Performance analysis of antennas (A_1–A_4).

Antenna	Port No.	Number of Bands	Operating band(GHz)/ Impedance BW (in %)	Isolation (dB)	Resonant frequency (GHz)	Reflection Coefficient (dB)	Peak Gain (dBi)
A1 	Port 1	1	20.21-23.42/14.7	<-22	20.24	-20.91	3
		2	24.71-27.82/11.8	<-22	25.22	-12.34	4
	Port 2	1	21.22-24.21/13.1	<-22	20.24	-21.01	3.5
		2	24.71-27.92/11.9	<-19	25.22	-12.34	4
A2 	Port 1	1	17.96-20.37/12.5	<-23	18.30	-18.41	4.8
		2	21.51-31.06/36.3	<-25	26.91	-22.21	5.5
	Port 2	1	18.21-20.37/13.5	<-25	18.30	-18.61	4.3
		2	21.51-31.06/36.3	<-25	26.91	-23.01	5.5
A3 	Port 1	1	19.10-26.72/33.2	<-29	24.71	-19.48	4.2
		2	27.12-31.01/13.3	<-27	26.91	-22.24	4.9
	Port 2	1	19.22-25.89/29.6	<-30	24.71	-19.33	4.4
		2	27.12-31.12/13.7	<-27	26.91	-22.20	4.6
A4 	Port 1	1	18.61-20.01/7.2	<-38	19.65	-15.91	6.5
		2	21.52-33.91/44.5	<-33	22.31	-15.90	8.1
	Port 2	1	18.61-20.01/7.2	<-38	19.65	-35.82	6.5
		2	21.52-33.91/44.5	<-33	22.31	-35.88	7.9

and measured analysis is < -35 dB (cf. Figure 6(a) and Table 1). Figure 6(b) clearly demonstrates peak gains 6.5 dBi and 8.1 dBi (simulated)/5.3 dBi and 7.7 dBi (measured) respectively for port-1 at resonating frequencies 19.65 GHz and 22.31 GHz. In Figure 6(b) and Table 1 it is observed that the peak gain (simulated and measured) effects are in slightly different at port-2 as compared to port-1.

4. PERFORMANCE PARAMETERS

To investigate the diversity performance of the MIMO antenna, metrics like ECC (envelope correlation coefficient), DG (diversity gain), TARC (total active reflection coefficient), and CLL (channel capacity loss) are reported in this section. The double flare horn shaped antenna offers an ECC lower than 0.005, DG greater than 9.996, TARC below -10 dB (simulated & measured), and channel capacity loss values are below 0.2 bits/sec/Hz (simulated and measured) as a utility of frequency is displayed in Figure 7.

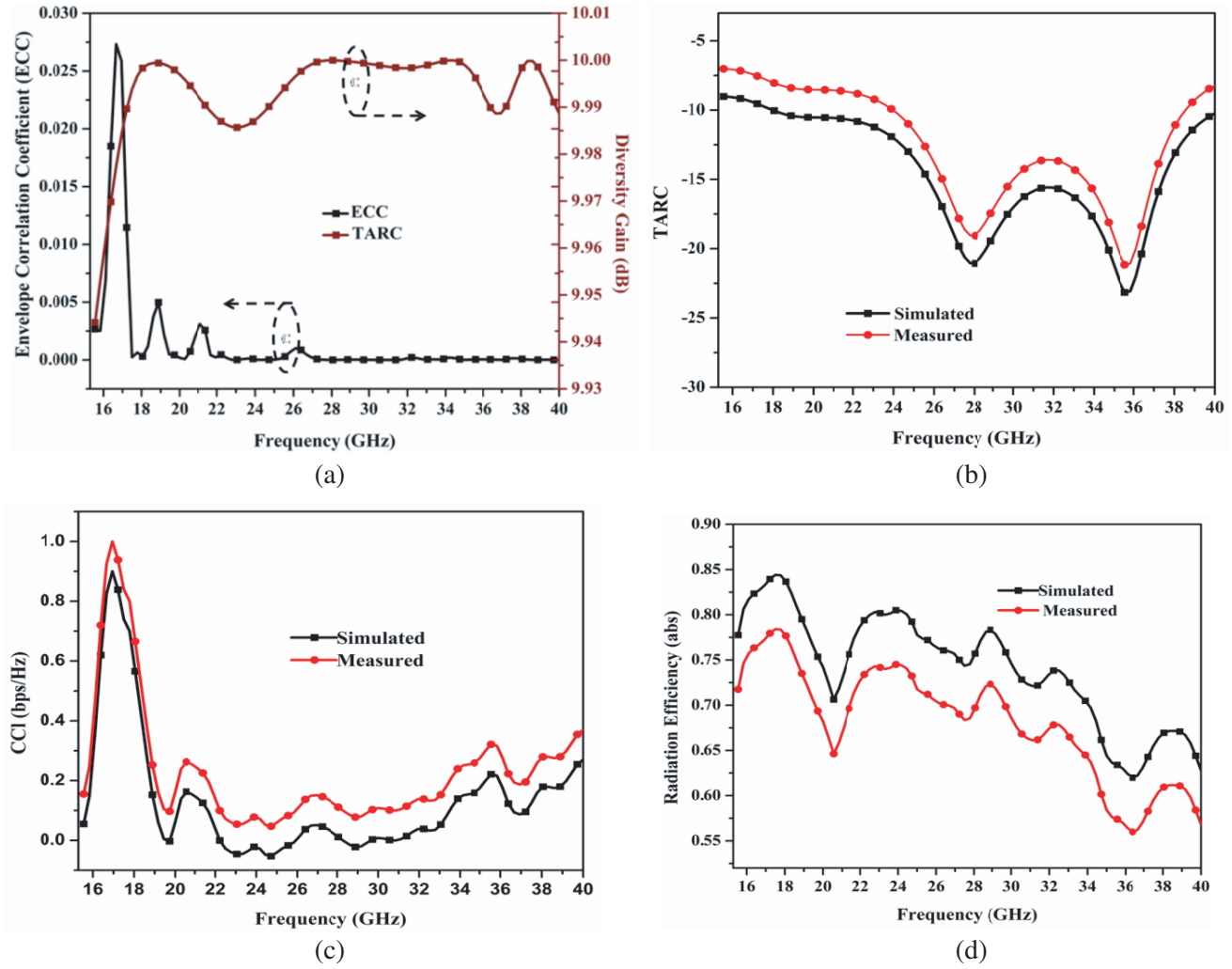

Figure 7. Analysis of Antenna A_4, (a) ECC & DG, (b) TARC (simulated and measured), (c) CCL (simulated and measured), (d) radiation efficiency (simulated and measured).

4.1. Envelope Correlation Coefficient (ECC)

Envelope correlation coefficient refers to the effect of one antenna on the performance of another. In other words, it assesses the influence of one unit cell on the performance of another unit cell. ECC of the antenna is given in Equation (1) to demonstrate how variation of the proposed antenna is in the acceptable limit (0–0.005) which conforms to the minimum isolation effect between antenna ports in this article (in Figure 7(a)) [19].

$$ECC = \frac{|S_{11} * S_{12} + S_{21} * S_{22}|}{\left(1 - |S_{11}|^2 - |S_{21}|^2\right)\left(1 - |S_{22}|^2 - |S_{12}|^2\right)} \tag{1}$$

4.2. Diversity Gain (DG)

Furthermore, the diversity gain is the process of the proposed antenna leads to the highest signal from a set of N signal, without increasing the input power level; the DG option enhances the signal-to-noise ratio. The following equation is used to compute it [20]. It can be obtained (in Figure 7(a)) the diversity gain in just able range between (9.99–10 dB)

$$\text{Diversity Gain} = 10 \times \sqrt{1 - (ECC)^2} \tag{2}$$

4.3. Total Active Reflection Coefficient (TARC)

To resolve the bandwidth & efficiency of MIMO antenna, the TARC (total active reflection coefficient) is e of the key factors. It is calculated by the sum of the ratio of square root of total reflected power to the square root of total incident power. Thus, the proposed TARC value is less than −10 dB (simulated and measured) for the entire band (Figure 7(b)) in this article [21].

$$\begin{matrix} t \\ a \end{matrix} = \frac{\Sigma_i^N |b_i|^2}{\Sigma_i^N |a_i|^2} \tag{3}$$

where a_i is the ith port forward wave amplitude, $[b] = [S][a]$, and for dual port MIMO antenna system, it is portrayed as,

$$\text{TARC} = \frac{(S_{11} + S_{12})^2 + (S_{22} + S_{21})^2}{\sqrt{2}} \tag{4}$$

4.4. Channel Capacity Loss (CCL)

For MIMO configuration, channel capacity is an important parameter to determine multiplexing and the equation in terms of return loss (S_{11} & S_{22}) & transmission coefficient (S_{12} & S_{21}) in Equation (5). The design has high isolation values greater than 35 dB in most of the band. In Figure 7(c), the channel capacity loss of the proposed antenna is less than 0.2 bits/sec/Hz (simulated & measured both) at the desired operating band. It is calculated by using Equation (5) for two port MIMO antenna.

$$\begin{aligned} CCL \;=\; & \log_2 \left[\left(\left(1 - |S_{11}|^2 - |S_{12}|^2\right) \left(1 - |S_{22}|^2 - |S_{21}|^2\right) \right) \right. \\ & \left. - \left(\left(S_{11} * S_{12} + S_{21} * S_{22}\right) \left(S_{22} * S_{21} + S_{12} * S_{11}\right) \right) \right] \end{aligned} \tag{5}$$

4.5. Radiation Efficiency

Figure 7(d) portrays the simulated and measured radiation efficiency plots of considered MIMO antenna more than 75% (simulated) & 70% (measured) for the entire resonating band of 18.61–20.01 GHz (simulated)/19.55–20.01 GHz (measured) and 21.52–33.91 GHz (simulated)/22.62–32.91 GHz (measured), respectively. For MIMO antenna when both port-1 and port-2 are excited, the antenna element port is kept terminated with 50 Ω impedance load. Anyhow, a tiny fluctuation is observed between the simulated & measured values, which may be due to soldering and fabrication leniency.

4.6. Electric Field Distribution, VSWR and Radiation Pattern

To decipher the confirmation of the double flare horn structure, electric field distribution (A/m) analysis is performed at two resonant frequencies of 19.65 GHz & 22.31 GHz with 54 A/m and 42 A/m respectively at port-1, and the same electric field distribution is observed at resonant frequency with port-2 in Figures 8(a) and (b). It can be seen that port-1 is excited to monitor the electric current distribution, thus port-1 is being prevented from the strong electric field of antenna port-2. It also clarifies that the separation between different ports is reported as the maximum surface electric field strength near the active port and the other ports are less disturbed by active port radiation. Figure 10 depicts the voltage standing wave ratio characteristic of the double flare horn structure, and it can be shown that the dual port MIMO antenna has a comparable VSWR of 1.52 (simulated) and 2.1 (measured) at 19.65 GHz and 1.51 (simulated) and 1.55 (measured) at 22.31 GHz with port-1, meeting the standard for VSWR < 2. The antenna features a $2:1$ VSWR and a bandwidth 15900 MHz (18.9–34.8 GHz).

Figure 9 illustrates as per the simulation and measurements, the recommended antenna's Co/Cross polarization patterns in both the E-plane & H-plane, when the elevation axis corresponds to the polar axis ($\theta = 0^\circ$) for the antenna's coordinate system. As a conclusion, the azimuth drive creates cuts at a consistent rate. Broadband horn was utilized as the fixed antenna (reference antenna). The elevation positioner was rotated in 5° increments from −180° to 180° for the prescribed measurement. The HFSS software and measurements were confiscated in an anechoic chamber. The main co-polar results are shown in Figure 9, which indicates good agreement between simulation & measurement. The test detecting may be allocated to the anechoic chamber's favoring hardware & gain inaccuracy in the

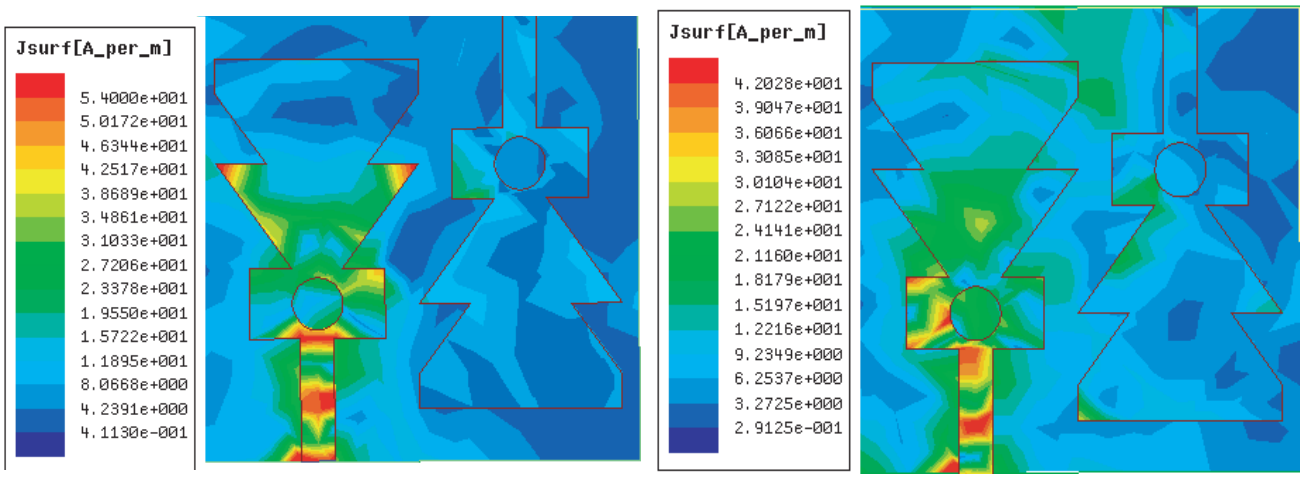

(a) (b)

Figure 8. Electric field distribution, (a) 19.65 GHz, (b) 22.31 GHz analysis of A_4 at port-1.

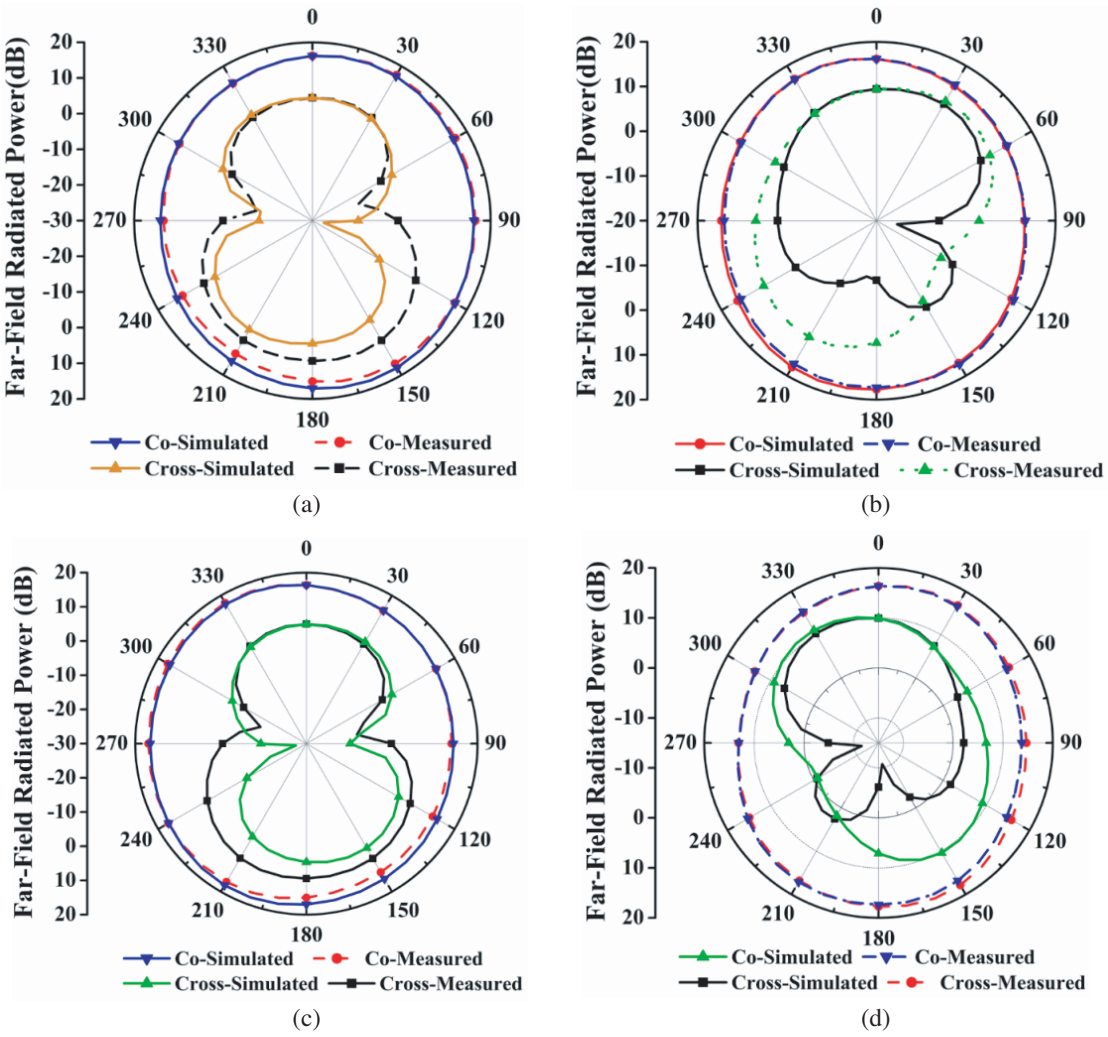

Figure 9. Co and Cross-polarization of the considered design in port-1, (a) *E*-plane at 19.65 GHz, (b) *H*-plane at 19.65 GHz, (c) *E*-plane at 22.31 GHz, (d) *H*-plane at 22.31 GHz.

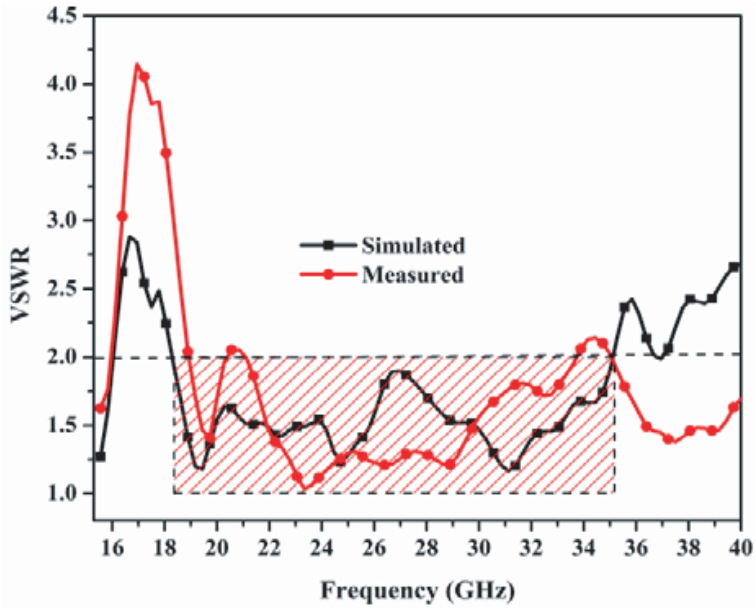

Figure 10. Analysis of VSWR (simulated and measured).

Table 2. Comparative analysis of the considered MIMO antenna.

Antenna size (mm^3)	No. of antennas	Operating band (GHz)/BW	Peak gain (dBi)	Isolation (dB)	ECC	DG (dB)	TARC (dB)	Radiation Efficiency (%)
$42 \times 85 \times 0.58$ [22]	2	27–32/5 (M)	7.9	−37.1	NR	NR	NR	80
$48 \times 21 \times 0.13$ [23]	2	29.5–31.5/2 (M)	7.1	−26	0.002	9.9	NR	NR
$30 \times 30 \times 0.0009$ [24]	4	27.5–29.5/2 (M)	5.8	−26	0.03	10	NR	90
$55 \times 50 \times 1.6$ [25]	2	15.31–20.02/4.7 25.6–35.21/9.6 (M)	7.5	−20	0.005	9.9	< 0	NR
$30 \times 52 \times 1.6$ [26]	2	2.0–3.6/1.6, 6.6–7.9/1.3, 9.6–12.7/3.1, 11–15.6/4.6 (M)	5, 3, 4.2, 6.6	−20, −40	0.024	9.9	< -9.96	NR
$30 \times 30 \times 1.6$ [27]	2	24.95–31.31/6.36 (S)	8.2 dBi	−15	0.0012	9.9	NR	70
$32 \times 20 \times 0.8$ [28]	2	3.3–7.8/4.5, 8.0-12.0/4 (M)	3	−20	0.05	9.8	< -10	69
$26 \times 26 \times 1.6$ (proposed work)	**2**	**18.61–20.01/1.4, 21.52–33.91/12.39 (M)**	**6.5, 8**	**-35**	**0.005**	**9.9**	**< -10**	**75**

ECC = Envelope Correlation Coefficient, DG = Diversity Gain,
NR = Not Reported, TARC = Total Active Reflection Coefficient,
BW = Bandwidth, M = Measured, S = Simulated

standard antenna used for the experiments. However, there were some inconsistencies in the radiation patterns detected. They are acceptable & negligible for mobile applications. Figure 9 also illustrates the equivalent findings for cross-polar patterns. These are less than 10–15 decibels compared to the co-polar patterns. While cross-polar components are undesirable & may induce uncertainty in MIMO systems, for many applications, a suppression level of 10–15 dB suffices.

4.7. Comparison of the Investigated Work with the Other Works

The comparative analysis of proposed MIMO antenna with other relative MIMO antennas is mentioned in Table 2 with reference to the size of antenna, number of ports, impedance bandwidth, peak gain, isolation, ECC, DG, & TARC.

5. CONCLUSION

In this communication, we have designed an ultra-wideband dual port MIMO antenna for the K and Ka bands of mm-wave application. The double flare horn structure has a compact design with a dimension of $0.19\lambda \times 0.19\lambda \times 0.01\lambda\,\mathrm{mm}^3$ at lower frequency. The proposed antenna A_4 is simulated using the HFSS EM simulator tools, and measurement is reported. Its results include an impedance bandwidth of 1.4 GHz (18.61–20.01) GHz and 1.23 GHz (21.52–33.91) GHz respectively at port $|S_{11}|$ and port $|S_{22}|$. However, port $|S_{22}|$ has the same resonant frequency as that at port $|S_{11}|$ with better isolation $|S_{21}| > 35$ dB within the S_{11} frequency range. At the resonant frequency, gains of 6.5 dBi & 8.1 dBi at port-1 and 6.5 dBi & 7.9 dBi at port-2 are observed, respectively. Additionally, the diversity performance of the antenna is analyzed in terms of the ECC (< 0.005), DG (9.9), TARC (< -10), & CCL (0.2 bits/sec/Hz).

REFERENCES

1. Pi, Z. and F. Khan, "An introduction to millimeter-wave mobile broadband systems," *IEEE Communications Magazine*, Vol. 49, No. 6, 101–107, 2011.
2. Rahimian, A. and F. Mehran, "RF link budget analysis in urban propagation microcell environment for mobile radio communication systems link planning," *2011 International Conference on Wireless Communications and Signal Processing (WCSP)*, 1–5, IEEE, November 2011.
3. Wang, C. X., F. Haider, X. Gao, X. H. You, Y. Yang, D. Yuan, and E. Hepsaydir, "Cellular architecture and key technologies for 5G wireless communication networks," *IEEE Communications Magazine*, Vol. 52, No. 2, 122–130, 2014.
4. Tan, C. M. and M. R. Tripathy, "A miniaturized T-shaped MIMO antenna for X-band and Ku-band applications with enhanced radiation efficiency," *2018 27th Wireless and Optical Communication Conference (WOCC)*, 1–5, IEEE, April 2018.
5. Pouyanfar, N., C. Ghobadi, J. Nourinia, K. Pedram, and M. Majidzadeh, "A compact multi-band MIMO antenna with high isolation for C and X bands using defected ground structure," *Radioengineering*, Vol. 27, No. 3, 686–693, 2018.
6. Li, Y., C. Wang, H. Yuan, N. Liu, H. Zhao, and X. Li, "A 5G MIMO antenna manufactured by 3-D printing method," *IEEE Antennas and Wireless Propagation Letters*, Vol. 16, 657–660, 2016.
7. Wang, Q., N. Mu, L. Wang, et al., "5G MIMO conformal microstrip antenna design," *Wireless Comms. and Mobile Computing*, 1–11, 2017.
8. Alhalabi, R. A. and G. M. Rebeiz, "High-efficiency angled-dipole antennas for millimeter-wave phased array applications," *IEEE Transactions on Antennas and Propagation*, Vol. 56, No. 10, 3136–3142, 2008.
9. Jilani, S. F. and A. Alomainy, "A multiband millimeter-wave 2-D array based on enhanced Franklin antenna for 5G wireless systems," *IEEE Antennas and Wireless Propagation Letters*, Vol. 16, 2983–2986, 2017.
10. Hussain, R., A. T. Alreshaid, S. K. Podilchak, and M. S. Sharawi, "Compact 4G MIMO antenna integrated with a 5G array for current and future mobile handsets," *IET Microwaves, Antennas & Propagation*, Vol. 11, No. 2, 271–279, 2017.
11. Wu, D., S. W. Cheung, T. I. Yuk, and X. L. Sun, "A planar MIMO antenna for mobile phones," *PIERS Proceedings*, 1150–1152, Taipei, March 25–28, 2013.
12. OuYang, J., F. Yang, and Z. M. Wang, "Reducing mutual coupling of closely spaced microstrip MIMO antennas for WLAN application," *IEEE Antennas and Wireless Propagation Letters*, Vol. 10, 310–313, 2011.

13. Chiu, C. Y., C. H. Cheng, R. D. Murch, and C. R. Rowell, "Reduction of mutual coupling between closely-packed antenna elements," *IEEE Transactions on Antennas and Propagation*, Vol. 55, No. 6, 1732–1738, 2007.
14. Chilukuri, S., K. Dahal, and A. Lokam, "Multi-port pattern diversity antenna for K and Ka-band application," *Advanced Electromagnetics*, Vol. 7, No. 2, 5–9, 2018.
15. Murali Krishna, C., M. Sai Prapoorna, K. Taruni Sesha Sai, and M. Sai Teja, "Super wideband 1×2 MIMO antenna for advanced wireless communication," *Advances in Electrical and Computer Technologies*, 509–519, Springer, Singapore, 2021.
16. Park, J. S., J. B. Ko, H. K. Kwon, B. S. Kang, B. Park, and D. Kim, "A tilted combined beam antenna for 5G communications using a 28-GHz band," *IEEE Antennas and Wireless Propagation Letters*, Vol. 15, 1685–1688, 2016.
17. Urimubenshi, F., D. B. Konditi, J. de Dieu Iyakaremye, P. M. Mpele, and A. Munyaneza, "A novel approach for low mutual coupling and ultra-compact two port MIMO antenna development for UWB wireless application," *Heliyon*, Vol. 8, No. 3, e09057, 2022.
18. Cicchetti, R., E. Miozzi, and O. Testa, "Wideband and UWB antennas for wireless applications: A comprehensive review," *International Journal of Antennas and Propagation*, 2017.
19. Dwivedi, A. K., A. Sharma, A. K. Singh, and V. Singh, "Circularly polarized quad-port MIMO dielectric resonator antenna with beam tilting feature for vehicular communication," *IETE Technical Review*, 1–13, 2020.
20. Dwivedi, A. K., A. Sharma, A. K. Singh, and V. Singh, "Metamaterial inspired dielectric resonator MIMO antenna for isolation enhancement and linear to circular polarization of waves," *Measurement*, Vol. 182, 109681, 2021.
21. Addepalli, T. and V. R. Anitha, "Compact two-port MIMO antenna with high isolation using parasitic reflectors for UWB, X and Ku band applications," *Progress In Electromagnetics Research C*, Vol. 102, 63–77, 2020.
22. Sehrai, D. A., M. Abdullah, A. Altaf, S. H. Kiani, F. Muhammad, M. Tufail, and S. Rahman, "A novel high gain wideband MIMO antenna for 5G millimeter wave applications," *Electronics*, Vol. 9, No. 6, 1031, 2020.
23. Rahman, S., X. C. Ren, A. Altaf, M. Irfan, M. Abdullah, F. Muhammad, and F. S. AlKahtani, "Nature inspired MIMO antenna system for future mmWave technologies," *Micromachines*, Vol. 11, No. 12, 1083, 2020.
24. Rappaport, T. S., Y. Xing, G. R. MacCartney, A. F. Molisch, E. Mellios, and J. Zhang, "Overview of millimeter wave communications for fifth-generation (5G) wireless networks — With a focus on propagation models," *IEEE Transactions on Antennas and Propagation*, Vol. 65, No. 12, 6213–6230, 2017.
25. Sharawi, M. S., S. K. Podilchak, M. T. Hussain, and Y. M. Antar, "Dielectric resonator based MIMO antenna system enabling millimetre-wave mobile devices," *IET Microwaves, Antennas & Propagation*, Vol. 11, No. 2, 287–293, 2017.
26. Saxena, G., P. Jain, and Y. K. Awasthi, "High diversity gain super-wideband single band-notch MIMO antenna for multiple wireless applications," *IET Microwaves, Antennas & Propagation*, Vol. 14, No. 1, 109–119, 2020.
27. Bhatia, S. S. and N. Sharma, "Modified spokes wheel shaped MIMO antenna system for multiband and future 5G applications: Design and measurement," *Progress In Electromagnetics Research C*, Vol. 117, 261–276, 2021.
28. Pandey, A., A. K. Singh, S. Singh, and R. Singh, "A compact Ultra-Wideband (UWB) MIMO antenna for K and Ka band applications," *IOT with Smart Systems*, 117–126, Springer, Singapore, 2022.